

Non-Uniformity of Non-Thermal Plasma Formation: Using FBG as Temperature Sensors

Siti Musliha Aishah Musa^{a,b,c}, Asrul Izam Azmi^c, Siti Azlida Ibrahim^a, Raja Kamarulzaman Raja Ibrahim^{b,*}

^a Faculty of Engineering, Multimedia University, 63100, Cyberjaya, Selangor, Malaysia

^b Faculty of Science, Universiti Teknologi Malaysia, 81310, Johor Bahru, Johor, Malaysia

^c Faculty of Electrical Engineering, Universiti Teknologi Malaysia, 81310, Johor Bahru, Johor, Malaysia

Corresponding author: *rkamarulzaman@utm.my

Abstract—This research investigates fiber Bragg grating (FBG) temperature sensing performance in monitoring non-uniformity of non-thermal plasma (NTP) formation in a packed-bed reactor using FBG operating at atmospheric pressure. Two FBGs made from germanium doped fiber were embedded inside and outside the PBNTTP reactor to allow for comparison between the temperatures inside and outside of the reactor to be made. Each FBG comes with three grating series, which allow the reactor temperatures at three different locations inside or outside the reactor to be measured and compared. Two types of plasma, namely nitrogen (N₂) and argon (Ar) were generated in the reactor at a gas flow rate in the range of 2 - 7 L/min and applied voltage in the range of 1 - 20 kV. It was found that the PBNTTP reactor temperature varies up to 20 °C at different positions inside and up to 40 °C outside of the reactor. This finding shows the non-uniformity of plasma formation and the nature of the plasma's localized thermodynamic equilibrium (LTE). The sensitivity of the FBG temperature sensor used in this study is estimated at 10.36 - 10.50 pm/°C.

Keywords—Fiber Bragg grating (FBG); temperature; fiber optic sensor; non-thermal plasma (NTP).

Manuscript received 21 Nov. 2022; revised 17 May 2023; accepted 21 Jul. 2023. Date of publication 31 Oct. 2023.
IJASEIT is licensed under a Creative Commons Attribution-Share Alike 4.0 International License.



I. INTRODUCTION

Fiber Bragg grating (FBG) is widely used in many applications, including telecommunication systems [1] and sensing purposes. In sensing applications, FBG has been used to monitor temperature [2]–[4], vibration [5], [6], pressure [7]–[9], strain [10]–[12] and acoustic [13], [14]. The vast sensing applications using FBG are due to its advantages, such as small sensor size, flexibility, non-electrical contact, immunity from electric and electromagnetic fields [15]–[17], and the ability to offer remote measurement with high-performance measurement. Using FBG, temperature measurement can be performed in harsh environments such as at radioactive radiation [18], electrical power systems [19], and elevated temperature [20], [21] and can also be used to measure localized and non-uniform temperature distribution measurements [22]. With these advantages, FBG can offer the best solution for monitoring packed-bed non-thermal plasma (PBNTTP) reactor temperature.

PBNTTP reactor generates plasma based on dielectric barrier discharge and has been used in many applications, including volatile organic compounds (VOCs) decomposition

[23], [24], thin film coating [25], [26], sterilization device [27] and degradation of pesticides [28]. High voltage is applied between two electrodes separated by a dielectric material, such as *barium titanate* BaTiO₃ [29]. The purpose of BaTiO₃ is to enhance the electric field between two electrodes. Carrier gas is introduced to generate plasma in an ionization process at breakdown voltage. This process generates cold or non-thermal plasma as electric energy, mostly channels to electrons instead of dissipating as thermal energy. However, a small fraction of electric energy is dissipated at particularly high voltage and causes PBNTTP reactor temperature to increase.

There are two important consequences of reactor temperature: first, it will influence the chemical reactions inside the reactor, and second, it can damage the reactor at very high temperatures. Therefore, the temperature of the PBNTTP reactor is of great importance and should be monitored and profiled. In this work, FBG was successfully demonstrated as a suitable device to perform temperature measurements for PBNTTP reactors.

A. Non-Thermal Plasma (NTP)

NTP, also known as cold or non-equilibrium plasma, can exist in low-pressure conditions [30]. The electron temperature of NTP can reach up to 10 000 K to 100 000 K, but the gas temperature can stay as low as room temperature. This means electrons gain very high kinetic energy from the electric field provided by high-voltage AC. These energetic electrons can be used to initiate and enhance many chemical processes through electron, molecule, or atom collision [31]. The techniques to produce NTP at atmospheric pressure include through dielectric discharge [32]–[34] and electron beams [35]. NTP also comes with several types of discharge that have been studied until today, such as glow [36], [37], corona [38], silent or dielectric barrier discharge (DBD) [39] radio frequency [40], microwave and, gliding arc [41]. This study uses a packed-bed non-thermal plasma (PBNT) reactor to generate glow discharge. A glow discharge, an electron, is a highly energetic particle operated between two perforated electrodes at low pressure [42]. Furthermore, glow discharge is stable at low pressure, which eases the reactor temperature.

B. Packed-Bed Non-Thermal Plasma Reactor (PBNT)

The packed-bed reactor is a combination of DBD and surface discharge. The dielectric bead material was packed inside the reactor to enhance the electric field in a range of 10 – 250 Vm^{-1} compared to the externally supplied source, as shown in Figure 1.

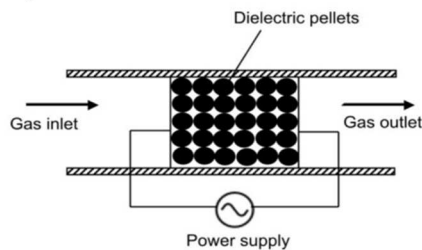


Fig. 1 A typical PBNT discharge reactor with dielectric beads

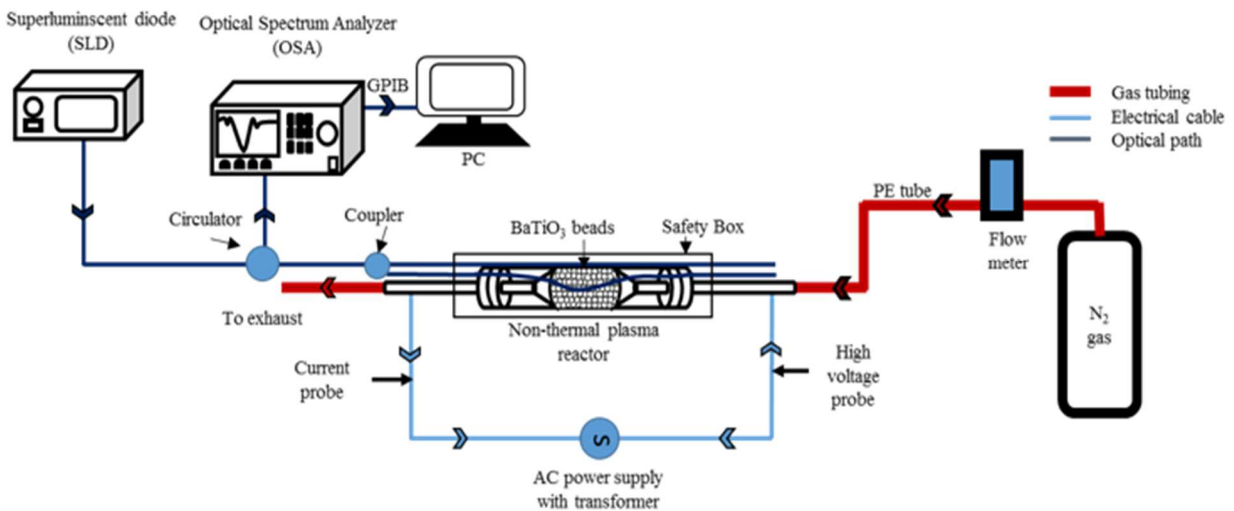


Fig. 2 PBNT reactor experimental setup

One end from each of FBG B and FBG C related to each of the output ports of the 1 x 2 coupler, while the input port was linked with the circulator's third port (blue wire). Port 1 is connected to SLD for the circulator, while Port 2 is

The beads refract, create non-uniformity, and produce an electric field with stronger beads depending on their setup. Non-thermal plasma is then formed in-between spaces of dielectric beads. In this work, barium titanate, BaTiO_3 was used as dielectric material discharge because it has high dielectric permittivity, ϵ [43].

PBNT reactors are widely used in pollution abatement in chemicals such as petrochemicals and petroleum. The reactor successfully improves the oxidation of organic air pollutants at lower concentrations. Placing a dielectric material such as perovskites requires low electric field power. It also modifies energy distribution by electron acceleration and controls reactive species in the reactor [44]. In addition, PBNT can also control air pollution. A study has shown that a reactor containing packed non-catalytic dielectric beads with specific energy density can obtain energy efficiency for ozone generation and gaseous pollutant abatement 1 -12 times higher in comparison to that of a non-packed reactor; depending on the type of pollutant, the reactor geometry, and the packing beads used [45]. The ferroelectric beads play important roles in the reactor performance as they can influence the distribution of electrons and the discharge length in the plasma on the various reactions [25].

II. MATERIAL AND METHOD

The whole setup of the reactor consists of three main components: the optical, electrical, and gas components. All these components were operated to measure real-time temperature outside and inside the PBNT reactor. The full setup of the experiment is presented in Figure 2. The FBG was designed and fabricated with a single grating and two triple gratings in series. The single FBG (FBG A) was used for characterization and preliminary experimental testing, while the triple grating FBGs were used to monitor the temperature profile outside (FBG B) and inside (FBG C) the reactor, as illustrated in Figure 3.

connected to the OSA. OSA was switched on and left for 5 minutes for warming-up purposes. The settings used for the OSA with an operating wavelength range of 1548.0 nm – 1562.0 nm, resolution at 0.07 nm, and bandwidth of 1 kHz.

SLD was then switched on and left for 5 minutes for warming-up purposes. The settings used for the SLD with an output power of 1.83 mW and Continuous Current (C.C). The PC should be ensured to have a continuous power supply (i.e., do not use a power supply from a battery for a laptop) to avoid the PC being damaged. General Purpose Interface Bus (GPIB) was secured with OSA and connected with PC by using USB. The following settings for temperature measurement were input into the LabVIEW program, which was readily installed in PC prior: wavelength range of 1548.0 nm – 1562.0 nm, threshold at -45 dBm, and width at 50 nm.

The high voltage and current probes were attached to the rod funnel PBNTTP reactor. Voltage and current data were recorded from the Pico scope and connected to a high-voltage and current probe. The flow meter was connected to the feed gas (N_2 or Ar) supply and the reactor via a polyethylene (PE) tube. For the first parameter, the flow rate of the gas was set as 5 SCFH (ft³/H), equivalent to 2.36 L/min. Immediately after the gas filled up the reactor, the initial temperature of the PBNTTP reactor was taken by using a digital thermocouple and input in LabVIEW program. This experiment was repeated with flow rates of 3.54, 4.72, 5.89 and 7.07 L/min. The feed gas was changed to Ar and was repeated for a flow rate of 2.36 L/min. The experiment was run again for flow rates of 3.54 and 4.72 L/min.

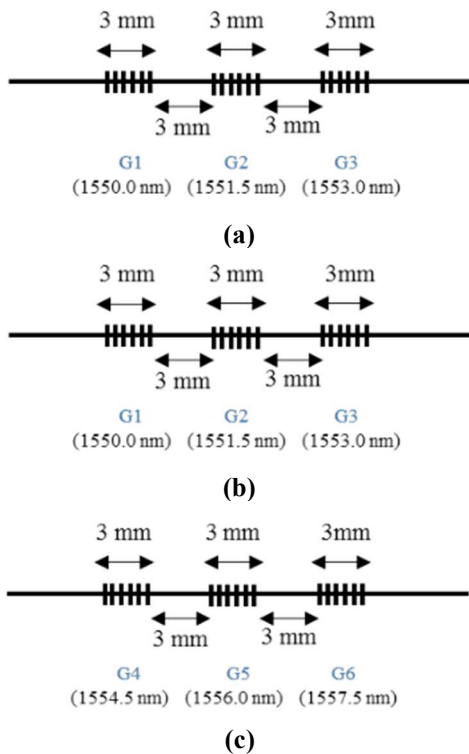


Fig. 3 (a) A single grating with 5mm length (FBG A), (b) triple grating with 3mm length each located outside (FBG B) & (c) inside PBNTTPR (FBG C)

III. RESULT AND DISCUSSION

A. Packed-Bed Non-Thermal Plasma (PBNTTP) Reactor Temperature Profile

The increase in N_2 plasma temperature outside and inside the PBNTTP reactor for 1 to 20 kV and a flow rate of 4.78 L/min is illustrated in Figure 4. From this graph, it can be observed that there is a large temperature gap between the outside and inside of the reactor and between each grating of

FBG. Gratings G1, G2, and G3 for FBG B positioned outside the reactor were arranged almost in parallel with gratings G4, G5, and G6 of FBG C on the inside. The maximum temperature gap between the outside and inside was 61.8 °C. The temperature inside PBNTTP reactor is higher than outside because the inside FBG has direct contact with the plasma stream while outside FBG is located outside the reactor. The reactor temperature started to change at 12 kV due to the formation of NTP. However, from the experiment data indicating specific early plasma ignition, only G1 at this moment could detect this temperature change due to plasma formation. It is believed that the NTP was first formed at a location inside the PBNTTP reactor that is closest to G1. This finding might suggest that plasma formation is localized.

The temperature profile of Ar plasma, as shown in Figure 5, is more uniform compared to N_2 plasma. As the voltage supply gradually increased, the temperature dropped slowly until 9.5 kV for all gratings except G1 (outside), which continued until 9.8 kV. This was because the NTP started to form at this point, and the heat was then held. By observation, the early formation of NTP inside the reactor is at 8 kV. However, the FBGs can only record the presence of NTP at 10 kV at G1 and the rest at 9.5 kV denoted via temperature rise, indicating specific early plasma ignition. The temperature gap between FBGs outside and inside is obviously separated at 10.3 kV, where NTP becomes brighter and occupies all space inside the PBNTTP reactor until 20 kV. The minimum gap between the outside and inside was 8 °C, while the maximum was 52.7 °C. However, temperature gaps between each grating are smaller, with a maximum of 11.5 °C inside and 10.9 °C outside. For cooling curves of N_2 and Ar plasma from both Figure 3 and Figure 4, it can be seen sharp decreases until almost room temperature by time duration ~ 400 s. The sensitivity of FBGs for temperature measurement was estimated in the range of 10.36 pm/ °C – 10.50 pm/ °C. The fast-cooling process proved that the plasma characteristic is local thermal equilibrium (LTE) compared to the water-cooling process, which needed almost 3600 s from boiling point to room temperature [46].

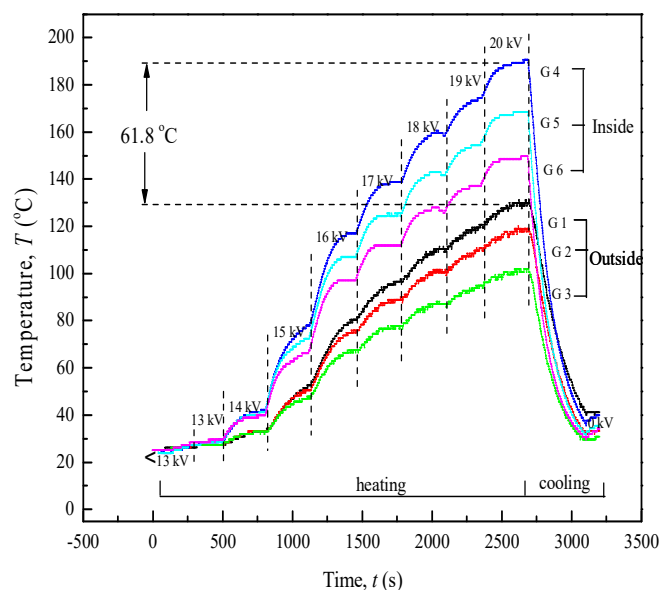


Fig. 4 Temperature profile outside and inside for every grating using N_2 plasma

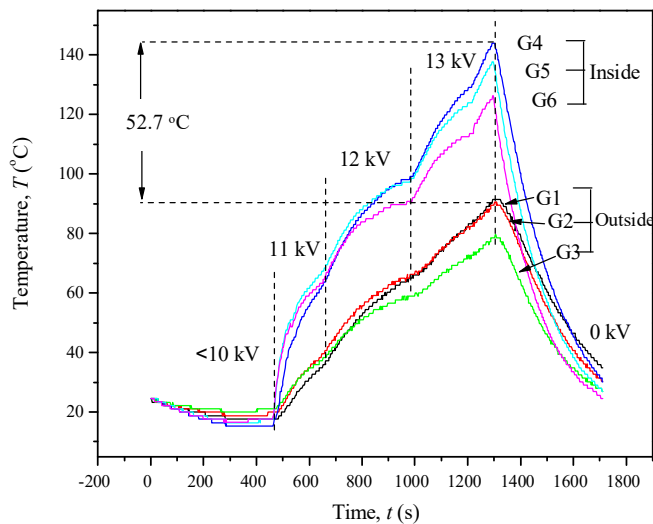


Fig. 5 Temperature profile outside and inside of reactor for every grating using Ar plasma

B. FBG Splitting

It was found that FBG spectrum recorded by OSA was splitting when the PBNTF reactor is operated at certain conditions, especially at very high supplied voltage. For example, the splitting was observed when the PBNTF reactor generated N_2 plasma with voltage slowly increased from 0 to 16 kV, and the flow rate was fixed at 4.78 L/min. In this case, a single Bragg grating, which is FBG A ($\lambda_B = 1541.1$ nm, grating's length = 5 mm, reflectivity = 90%) was used to record the PBNTF temperature reactor. The FBG spectra at different temperature is shown in Figure 6.

From the graph, at 25 to 30 °C there is no splitting of FBG spectrum. At this moment, FBG expansion is more uniform since the temperature is still low. At 40 °C, FBG spectrum started to split since there are different temperatures at a grating location, so FBG does not expand uniformly. Then, spectra splitting was clearly recorded at 50 °C and 60 °C. When the stress is minimal, the effect is that the Bragg wavelength experiences only a small shift in the X-polarization direction, resulting in a low intensity of the reflected peak. However, the Bragg peak exhibits a higher intensity in the Y-polarization direction.

Consequently, the Bragg peaks in the X direction are significantly impacted by those in the Y direction [47]. This condition is hard to explain because the real location of FBG cannot be proven, so assume it to be as shown in Figure 7. There are two possibilities of FBG spectrum splitting: plasma is not uniform, and UV emitting of plasma formation. It was found that N_2 plasma was not uniform and very localized, so 5 mm FBG's grating can detect two or more different temperatures. The UV from plasma formation is also considered because the fabrication of FBG uses a UV laser with a certain amount to create a grating [48]. In this case, the UV is not emitting enough to restructure the grating permanently. However, it may have temporarily changed the conditions on a portion of the FBG, leading to the splitting of temperature curves. The next sub-section will discuss how sufficient UV emission can permanently change the grating.

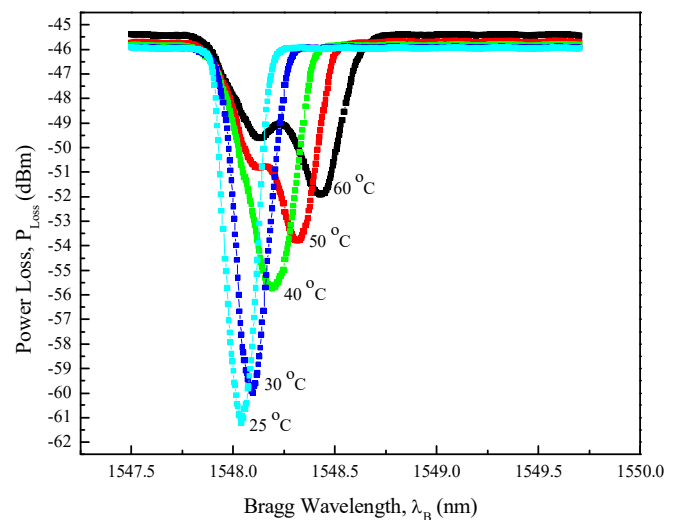


Fig. 6 FBG spectra at different temperatures when using 5mm single FBG grating

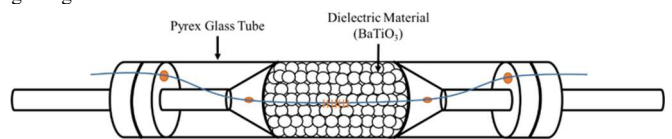


Fig. 7 Possible condition occurs inside PBNTF reactor due to splitting of FBG spectrum

C. Effect UV on FBG

PBNTF reactor generated toluene plasma with voltage increased from 0 to 18 kV and flow rate was fixed at 4.78 L/min. In this case, a single grating with Bragg wavelength of 1548.1 nm, 5 mm grating length, 90 % reflectivity was used to record PBNTF temperature reactor. The increasing of very high supplied voltage disturbed since air molecules emitted enough UV [31] to change the FBG's grating permanently, as shown in Figure 8. This phenomenon is called photobleaching. FBGs can undergo photobleaching when exposed to intense UV light for an extended period. Photobleaching refers to the reduction or erasure of the refractive index modulation in the grating structure due to breaking bonds or photochemical reactions [49]. This can decrease the grating's reflectivity and a corresponding shift in the Bragg wavelength [50]. The Optical Emission Spectroscopy (OES) result proved UV produced during plasma formation depicted in Figure 9.

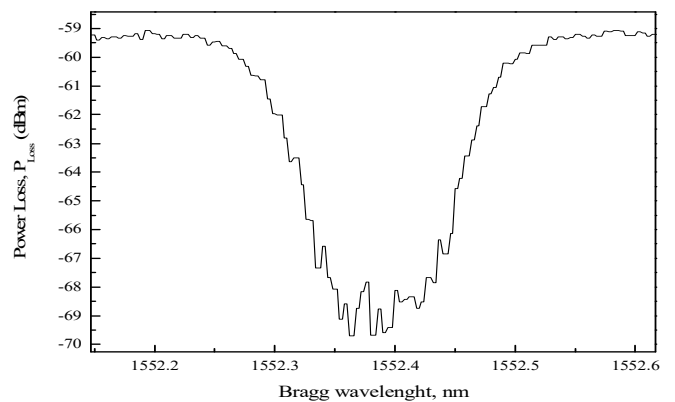


Fig. 8 FBG spectrum by using air plasma

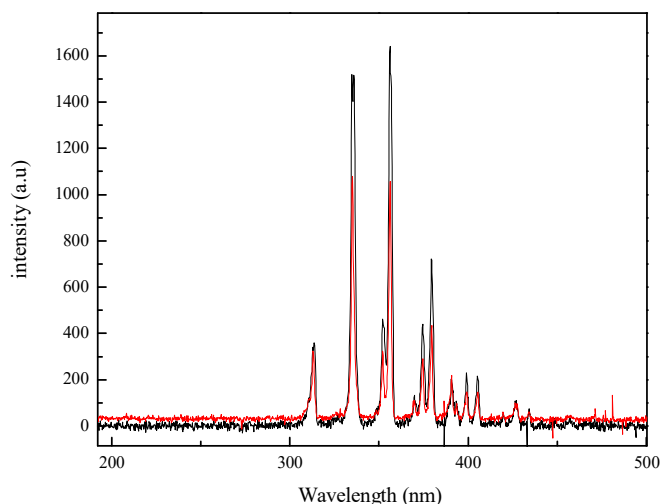


Fig. 9 UV emission during formation of plasma by using OES

IV. CONCLUSION

In this study, we explored the application of Fiber Bragg Gratings (FBGs) as temperature sensors for monitoring the non-uniformity of non-thermal plasma (NTP) formation within a packed-bed reactor. The study encompassed the generation of two types of plasma, nitrogen (N_2) and argon (Ar), within the reactor, with gas flow rates ranging from 2 to 7 L/min and applied voltages spanning 1 to 20 kV. It was observed that the temperature within the packed-bed non-thermal plasma (PBNTP) reactor exhibited significant disparities, with fluctuations of up to 20°C at various positions inside and up to 40°C outside of the reactor. This variability underscored the non-uniformity of plasma formation and the localized thermodynamic equilibrium (LTE) character of the plasma. The FBG temperature sensor employed in this investigation exhibited a sensitivity estimated between $10.36\text{ pm}/^\circ\text{C}$ and $10.50\text{ pm}/^\circ\text{C}$. This precision in temperature measurement proved invaluable for monitoring the temperature fluctuations associated with PBNTP reactors and the distinctive characteristics of NTP formation. This research sheds light on the promising utility of FBG sensors in the field of non-thermal plasma research, offering insights into the non-uniformity of plasma generation and its potential implications. The findings have significant implications for the optimization and control of PBNTP reactors, with potential applications in areas such as pollutant abatement, thin film coating, and sterilization. Furthermore, the observed FBG splitting phenomenon and its relationship with UV emission contribute to a deeper understanding of the mechanisms at play within these reactors. In summary, the utilization of FBGs as temperature sensors provides a powerful tool for characterizing and understanding the dynamics of non-thermal plasma formation, and it represents a vital advancement in the field of plasma science and technology. Further research and exploration are warranted to harness the full potential of this technology for various applications.

ACKNOWLEDGMENTS

This work was supported by Universiti Teknologi Malaysia (Q.J130000.2554.20H97), Telekom Malaysia Research Fund (Project number: RDTTC/221043), and MMU

postdoctoral researcher fund (MMUI/220125, MMUI/230002).

REFERENCES

- [1] A. Othonos, K. Kalli, and G. E. Kohnke, "Fiber Bragg Gratings: Fundamentals and Applications in Telecommunications and Sensing," *Phys Today*, vol. 53, no. 5, pp. 61–62, May 2000, doi: 10.1063/1.883086.
- [2] S. Daud, M. A. Jalil, S. Najmee, S. Saktioto, J. Ali, and P. P. Yupapin, "Development of FBG sensing system for outdoor temperature environment," in *Procedia Engineering*, 2011, pp. 386–392. doi: 10.1016/j.proeng.2011.03.071.
- [3] A. L. Voloshina, A. A. Dmitriev, S. V. Varzhel, and V. A. Kulikova, "Development and investigation of the sensitive element of the amplitude fiber-optic temperature sensor based on superimposed chirped Bragg gratings," *Optical Fiber Technology*, vol. 75, Jan. 2023, doi: 10.1016/j.yofte.2022.103175.
- [4] H. Wang *et al.*, "Fast response characteristics of fiber Bragg grating temperature sensors and explosion temperature measurement tests," *Sens Actuators A Phys*, vol. 354, May 2023, doi: 10.1016/j.sna.2023.114236.
- [5] G. Cazzulani, S. Cinquemani, L. Comolli, A. Gardella, and F. Resta, "Vibration control of smart structures using an array of Fiber Bragg Grating sensors," *Mechatronics*, vol. 24, no. 4, pp. 345–353, 2014, doi: 10.1016/j.mechatronics.2013.07.014.
- [6] Z. Jia *et al.*, "A two-dimensional cantilever beam vibration sensor based on fiber Bragg Grating," *Optical Fiber Technology*, vol. 61, Jan. 2021, doi: 10.1016/j.yofte.2020.102447.
- [7] Q. Shu, L. Wu, S. Lu, and W. Xiao, "High-sensitivity structure based on fiber Bragg grating sensor and its application in nonintrusive detection of pipeline pressure change," *Measurement (Lond)*, vol. 189, Feb. 2022, doi: 10.1016/j.measurement.2021.110444.
- [8] A. F. Stephens, A. Busch, R. F. Salamonsen, S. D. Gregory, and G. D. Tansley, "A novel fibre Bragg grating pressure sensor for rotary ventricular assist devices," *Sens Actuators A Phys*, vol. 295, pp. 474–482, Aug. 2019, doi: 10.1016/j.sna.2019.06.028.
- [9] H. Kumar, M. N. Sreerangaraju, and P. Sharan, "Characterization of Hydroacoustic Optical Fibre Bragg Grating Pressure Sensor Using Different Materials," *Results in Optics*, vol. 2, Jan. 2021, doi: 10.1016/j.rio.2020.100037.
- [10] F. Mashayekhi, J. Bardon, Y. Koutsawa, S. Westermann, and F. Addiego, "Methods for embedding fiber Bragg grating sensors during material extrusion: relationship between the interfacial bonding and strain transfer," *Addit Manuf*, p. 103497, Apr. 2023, doi: 10.1016/j.addma.2023.103497.
- [11] W. Li, S. Chen, Y. Chu, P. Huang, and G. Yan, "Wide-range fiber Bragg grating strain sensor for load testing of aircraft landing gears," *Optik (Stuttg)*, vol. 262, Jul. 2022, doi: 10.1016/j.ijleo.2022.169290.
- [12] Z. Zhou, J. He, Y. Zhang, J. Yu, and S. Zhang, "Development and performance study of fiber Bragg grating flexible cable strain sensor," *Optik (Stuttg)*, vol. 273, Feb. 2023, doi: 10.1016/j.ijleo.2023.170505.
- [13] F. Yu, Z. Li, and Y. Okabe, "Application of a remotely bonded fiber-optic Bragg grating sensor to acoustic emission testing for a carbon-carbon composite at a temperature of 1000°C ," *Measurement (Lond)*, vol. 203, Nov. 2022, doi: 10.1016/j.measurement.2022.111908.
- [14] F. Yu and Y. Okabe, "Linear damage localization in CFRP laminates using one single fiber-optic Bragg grating acoustic emission sensor," *Compos Struct*, vol. 238, Apr. 2020, doi: 10.1016/j.compstruct.2020.111992.
- [15] R. Montanini and S. Pirrotta, "A temperature-compensated rotational position sensor based on fibre Bragg gratings," *Sens Actuators A Phys*, vol. 132, no. 2, pp. 533–540, Nov. 2006, doi: 10.1016/j.sna.2006.02.036.
- [16] Sheng Kai Lin *et al.*, "The Fabricating the UV polymer Bragg grating on the D- shaped fiber," in *2010 International Conference on Optics, Photonics and Energy Engineering*, Institute of Electrical and Electronic Engineers, 2010, pp. 14–17.
- [17] Ming Fu Zhao, Shao Fei Wang, Bin Bin Luo, Nian Bing Zhong, and Xue Mei Cao, "Theoretical study on the cross sensitivity of fiber Bragg grating sensor affected by temperature and transverse pressure," in *2010 Symposium on Photonics and Optoelectronics*, IEEE, 2010, pp. 1–4.
- [18] A. Morana *et al.*, "Radiation Effects on Fiber Bragg Gratings: Vulnerability and Hardening Studies," *Sensors*, vol. 22, no. 21. MDPI, Nov. 01, 2022. doi: 10.3390/s22218175.

- [19] H. A. Gabbar and Y. Elsayed, "Application of Fiber Bragg Gating (FBG) Sensing Technologies in Power Systems," *IEEE Smart Grid*, pp. 1–7, 2021.
- [20] J. Canning *et al.*, "Optical fibre Bragg gratings for high temperature sensing," in *20th International Conference on Optical Fibre Sensors*, SPIE, Oct. 2009, p. 75032N. doi: 10.1117/12.834470.
- [21] J. He *et al.*, "Stabilized Ultra-High-Temperature Sensors Based on Inert Gas-Sealed Sapphire Fiber Bragg Gratings," *ACS Applied Materials & Interfaces*, vol. 14, no. 10, pp. 12359–12366, Feb. 2022, doi: 10.1021/acsami.1c24589.
- [22] L. Q. Yu, A. I. Azmi, S. M. A. Musa, and R. K. R. Ibrahim, "Application of packaging technique in Fiber Bragg Grating temperature sensor for measuring localized and nonuniform temperature distribution," *Jurnal Teknologi (Sciences and Engineering)*, vol. 64, no. 3, 2013, doi: 10.11113/jt.v64.2084.
- [23] W. Mista and R. Kacprzyk, "Decomposition of toluene using non-thermal plasma reactor at room temperature," *Catal Today*, vol. 137, no. 2–4, pp. 345–349, Sep. 2008, doi: 10.1016/j.cattod.2008.02.009.
- [24] S. K. P. Veerapandian, N. De Geyter, J. M. Giraudon, J. F. Lamonnier, and R. Morent, "The use of zeolites for VOCs abatement by combining non-thermal plasma, adsorption, and/or catalysis: A review," *Catalysts*, vol. 9, no. 1. MDPI, Jan. 01, 2019, doi: 10.3390/catal9010098.
- [25] A. Nasonova, H. C. Pham, D. J. Kim, and K. S. Kim, "NO and SO₂ removal in non-thermal plasma reactor packed with glass beads-TiO₂ thin film coated by PCVD process," *Chemical Engineering Journal*, vol. 156, no. 3, pp. 557–561, Feb. 2010, doi: 10.1016/j.cej.2009.04.037.
- [26] A. Iadicicco, S. Campopiano, A. Cutolo, M. Giordano, and A. Cusano, "Self temperature referenced refractive index sensor by non-uniform thinned fiber Bragg gratings," *Sens Actuators B Chem*, vol. 120, no. 1, pp. 231–237, Dec. 2006, doi: 10.1016/j.snb.2006.02.027.
- [27] T. Kuwahara, T. Kuroki, K. Yoshida, N. Saeki, and M. Okubo, "Development of sterilization device using air nonthermal plasma jet induced by atmospheric pressure corona discharge," in *Thin Solid Films*, Nov. 2012, pp. 2–5. doi: 10.1016/j.tsf.2012.05.064.
- [28] N. N. Misra, S. K. Pankaj, T. Walsh, F. O'Regan, P. Bourke, and P. J. Cullen, "In-package nonthermal plasma degradation of pesticides on fresh produce," *J Hazard Mater*, vol. 271, pp. 33–40, 2014, doi: 10.1016/j.jhazmat.2014.02.005.
- [29] N. Z. R. R. K. R. Ibrahim, S. M. A. Musa, R. H. S. A. I. Azmi, and N. Ahmad, "Reactor temperature profiles of non-thermal plasma reactor using fiber Bragg grating sensor," *Sensors and Actuators A*, vol. 244, pp. 206–212, 2016, doi: 10.1016/j.sna.2016.04.015.
- [30] V. Nehra, A. Kumar, and H K Dwivedi, "Atmospheric Non-Thermal Plasma Sources," in *International Journal of Engineering*, 2008, pp. 53–68.
- [31] J. P. Boeuf, L. C. Pitchford, A. Fiala, and P. Belenguer, "Modelling of discharges and non-thermal plasmas-applications to plasma processing," *Surf Coat Technol*, vol. 59, pp. 32–40, 1993.
- [32] Sameer U. Kalghatgi, Gregory Fridman, Alexander Fridman, Gary Friedman, and Alisa Morss Clyne, "Non-Thermal Dielectric Barrier Discharge Plasma Treatment of Endothelial Cells," in *30th Annual International IEEE EMBS Conference*, IEEE, 2008, pp. 3578–3581.
- [33] S. Li, X. Dang, X. Yu, G. Abbas, Q. Zhang, and L. Cao, "The application of dielectric barrier discharge non-thermal plasma in VOCs abatement: A review," *Chemical Engineering Journal*, vol. 388. Elsevier B.V., May 15, 2020. doi: 10.1016/j.cej.2020.124275.
- [34] J. Zhang, T. Kwon, S. Kim, and D. Jeong, "Plasma Farming: Non-Thermal Dielectric Barrier Discharge Plasma Technology for Improving the Growth of Soybean Sprouts and Chickens," *Plasma*, vol. 1, no. 2, pp. 285–296, Dec. 2018, doi: 10.3390/plasma1020025.
- [35] Q. Wei, J. Mei, and J. Xie, "Application of electron beam irradiation as a non-thermal technology in seafood preservation," *LWT*, vol. 169. Academic Press, Nov. 01, 2022. doi: 10.1016/j.lwt.2022.113994.
- [36] H. M. Valencia, F. B. Yousif, A. Robledo-Martínez, and F. C. Mejía, "Optical and electrical characteristics of AC glow-discharge plasma in N₂O," *IEEE Transactions on Plasma Science*, vol. 34, no. 4 III, pp. 1497–1502, Aug. 2006, doi: 10.1109/TPS.2006.877251.
- [37] K. Matsumoto, "Plasma production by multi-phase AC glow discharge at the frequency of a commercial electric power system," 1996. [Online]. Available: <http://iopscience.iop.org/0963-0252/5/2/018>
- [38] T. Hammer, "Atmospheric Pressure Plasma Application for Pollution Control in Industrial Processes," *Contributions to Plasma Physics*, vol. 54, no. 2, pp. 187–201, Feb. 2014, doi: 10.1002/ctpp.201310063.
- [39] D. H. Kim, Y. S. Mok, and S. B. Lee, "Effect of temperature on the decomposition of trifluoromethane in a dielectric barrier discharge reactor," in *Thin Solid Films*, Aug. 2011, pp. 6960–6963. doi: 10.1016/j.tsf.2010.11.060.
- [40] J. S. Kim, E. J. Lee, E. H. Choi, and Y. J. Kim, "Inactivation of *Staphylococcus aureus* on the beef jerky by radio-frequency atmospheric pressure plasma discharge treatment," *Innovative Food Science and Emerging Technologies*, vol. 22, pp. 124–130, 2014, doi: 10.1016/j.ifset.2013.12.012.
- [41] A. Fridman, S. Nester, L. A. Kennedy, A. Saveliev, and O. Mutaf-Yardimci, "Gliding Arc Discharge (GAD) Experiment," *Prog Energy Combust Sci*, vol. 25, pp. 211–231, 1999.
- [42] C.-J. Liu, G.-H. Xu, and T. Wang, "Non-thermal plasma approaches in CO utilization," *Fuel Processing Technology*, vol. 58, pp. 119–134, 1999.
- [43] Raja Kamarulzaman Raja Ibrahim, "Mid-Infrared Diagnostics of the Gas Phase in Non-Thermal Plasma Application," 2011.
- [44] U. Roland, F. Holzer, and F.-D. Kopinke, "Improved oxidation of air pollutants in a non-thermal plasma," *Catal Today*, vol. 73, pp. 315–323, 2002.
- [45] H. L. Chen, H. M. Lee, S. H. Chen, and M. B. Chang, "Review of packed-bed plasma reactor for ozone generation and air pollution control," *Ind Eng Chem Res*, vol. 47, no. 7, pp. 2122–2130, Apr. 2008, doi: 10.1021/ie071411s.
- [46] Bwei Zhang and M. Kahrizi, "Characteristics of fiber Bragg grating temperature sensor at elevated temperatures," in *2005 International Conference on MEMS, NANO and Smart Systems*, IEEE, pp. 241–246. doi: 10.1109/ICMENS.2005.33.
- [47] J. Xiong *et al.*, "Spectral Splitting Sensing Using Optical Fiber Bragg Grating for Spacecraft Lateral Stress Health Monitoring," *Applied Sciences*, vol. 13, no. 7, p. 4161, Mar. 2023, doi: 10.3390/app13074161.
- [48] R. Kashyap, "Introduction," in *Fiber Bragg Gratings*, Elsevier, 2010, pp. 1–13. doi: 10.1016/B978-0-12-372579-0.00001-6.
- [49] C. G. Askins and M. A. Putnam, "Photodarkening and photobleaching in fiber optic Bragg gratings," *Journal of Lightwave Technology*, vol. 15, no. 8, pp. 1363–1370, 1997, doi: 10.1109/50.618343.
- [50] J. Fiebrandt, S. Jetschke, M. Leich, M. Rothhardt, and H. Bartelt, "UV-induced photodarkening and photobleaching in UV-femtosecond-pulse-written fibre Bragg gratings," *Laser Phys Lett*, vol. 10, no. 8, p. 085102, Aug. 2013, doi: 10.1088/1612-2011/10/8/085102.